

A Novel Dual Predictors Framework of PEE

1st Fangjian Shen

dept. name of organization (of Aff.)

name of organization (of Aff.)

City, Country

email address or ORCID

1st Yicheng Zheng

dept. name of organization (of Aff.)

name of organization (of Aff.)

City, Country

email address or ORCID

1st Songyou Li

dept. name of organization (of Aff.)

name of organization (of Aff.)

City, Country

email address or ORCID

Abstract—This document is a model and instructions for \LaTeX . This and the `IEEEtran.cls` file define the components of your paper [title, text, heads, etc.]. *CRITICAL: Do Not Use Symbols, Special Characters, Footnotes, or Math in Paper Title or Abstract.

Index Terms—component, formatting, style, styling, insert

I. INTRODUCTION

With the rapid development of information technology and the widespread use of digital media, the security and confidentiality of digital information have become increasingly important. Data hiding, as a covert communication technology that embeds secret information in digital media, has been applied to more and more fields [8]–[10]. However, in the domains of digital copyright protection, telemedicine diagnosis, and military communication, it is essential that the original media can be fully recovered without any loss of information after extracting the secret information. Therefore, reversible data hiding (RDH) has garnered significant attention in the research community [16], [17] and has witnessed rapid development in recent years.

Currently, the two primary methods for reversible data hiding are **difference expansion (DE)** and **histogram shifting (HS)**. DE achieves it by modifying the difference between neighboring pixel values in the image [12], but the bit per pixel (bpp) of this method is low and the distortion is large. Whereas the HS algorithm [13]–[15] shifts the zero point of the histogram to the peak point and embeds confidential information into the corresponding bins. Nevertheless, the quality of the embedded image is constrained by the positional relationship between the peak and zero point. To address these limitations, **prediction-error expansion (PEE)** [4]–[7] was proposed in subsequent research.

PEE employs a specific predictor to obtain the prediction value based on the context of each pixel. It then subtracts the prediction value from the original pixel value to derive prediction-error. By counting the frequency of the prediction error, **prediction error histogram (PEH)** is generated. Compared to the pixel histogram, PEH takes advantage of the similarity between image pixels. So PEH has higher peaks, which results in larger embedding capacity (EC) and less distortion. Different from HS, which shifts between peaks and zeros, PEE selects bins -1 and 0 for expansion while shifting the other bins accordingly to ensure reversibility.

However, the choice of bins -1 and 0 for expansion in PEE does not always guarantee minimum distortion when capacity is low. Moreover, the prediction accuracy tends to decrease on images with drastic gray-scale changes, leading to dispersed PEH where the peak bin may not be located at 0 or -1. To overcome these challenges, later research introduced **PEE with optimal expansion bins selection (O-PEE)** [18], [19], which adaptively determines the expansion bins that minimize distortion while satisfying embedding capacity through exhaustive search, making it more effective than PEE. Additionally, **PEE with adaptive embedding (A-PEE)** [20]–[23] introduces complexity to measure drastic content of each pixel’s context changes. Since high complexity often results in high prediction error, A-PEE reduces distortion by filtering out pixels with high complexity, which makes the distribution of PEH sharper for less histogram shifts. Combining the advantages of both A-PEE and O-PEE, **PEE which combines both adaptive embedding and optimal expansion bins selection (AO-PEE)** [24], [25] achieves superior results. Furthermore, pairwise PEE extends PEH to two-dimensional (2D) PEH by counting prediction-errors of pixel pairs on the diagonal of mutually disjoint 2×2 pixel blocks. It adaptively discards mapping directions with large distortion, which not only obtains good embedding performance but also garners high capacity.

Unlike AO-PEE, which directly filters out pixels with high complexity, in [3], Li et al. proposed **multiple histogram modification (MHM)**, where complexity of each pixel is determined by summing both horizontal and vertical absolute differences of every two consecutive pixels in the context of each pixel. Then pixels will be divided into several intervals, and we generate PEH for each interval. Expansion bins are adaptively selected for each PEH, enabling efficient utilization of pixels with varying complexity levels. MHM can be considered a generalization of AO-PEE: when the histograms corresponding to high complexity classes remain unchanged and the expansion bins for low complexity ones are the same, MHM is equivalent to AO-PEE. Compared with AO-PEE, MHM significantly improved peak signal-to-noise ratio (PSNR).

Afterwards, many researchers have made further improvements to MHM. **Optimal MHM**, proposed by Qi et al. in [2], addresses the optimization problem of expansion bins selection by continuously reducing the original problem to smaller sub-

problems. In [1], Ou et al. introduced **high-capacity MHM**, which implements high capacity embedding by selecting multiple pairs of expansion bins for each PEH. Additionally, in [28] proposed by Xiao et al. , the prediction residual is calculated by removing the rounding operation to replace the prediction-error, and **prediction residual histogram(PRH)** is derived. Then they designed a new mapping mechanism to generate more expansion bins based on the PRH. To achieve higher image quality when embedding secret message, MHM is combined with PRE to get MHM-PRE, which surpasses previous MHM-like algorithms in terms of image quality.

The sharpness of PEH determines the final image quality, but the distribution of the PEH is closely related to the performance of predictor. Consequently, numerous research efforts have focused on enhancing the accuracy of predictors. The most widely used predictor is the rhombus predictor [27], which has proven effective in generating sharp PEH to achieve a better embedding result. However, adopting only one predictor is not always reliable. The prediction capability of one single predictor is inevitably confined, accurately predicting certain points while introducing biases in the prediction for other points.

In this paper, we propose an improved 2D-PEH by employing distinct predictors for prediction. If both of them have high prediction accuracy and low correlation, they can discriminate between different categories of pixel points. Unlike pairwise PEE, which uses the same predictor for pixel pairs on the diagonal of mutually disjoint 2×2 pixel blocks. Our proposed algorithm utilizes two distinct predictors for the same pixel to obtain double prediction-errors, and establishes 2D double prediction-error histogram (2D-DPEH) by counting the frequencies of them. The generated 2D-DPEH can be regarded as consisting of 1D-PEHs. Then for each 1D-PEH, we have to select the expansion bins separately. In 1, our proposed 2D-DPEH distribution, based on double prediction-errors, exhibits sharper feature compared to pairwise PEE on both Lena (plot with smooth gray-scale changes) and Baboon (plot with drastic gray-scale changes). What's more, in order to enhance the speed and performance of proposed method, the selection of expansion bins is determined by dynamic programming (DP) instead of exhaustive search. Finally, as an extension of some existing methods, we confirm the feasibility and superiority of the proposed scheme by combining 2D-DPEH with C-PEE and MHM.

The remaining parts of the paper is as follows. Some PEE-related methods are briefly introduced in II. Then the details of proposed method is presented in III, and the experimental results are shown in IV. Finally, V gives the conclusion.

II. RELATED WORK

A. C-PEE

The method based on the PEE framework consists of three steps: generating PEH, embedding, extracting and recovering. In C-PEE, a double-layered embedding scheme is adopted, which is to ensure reversibility in the case of utilizing rhombus predictor. This mechanism is to divide the set S consisting of

the cover image pixels into two subsets S_1 and S_2 as shown in Figure 2,

where S_1 for blue pixels and S_2 for yellow ones as $S_1 \cap S_2 = \emptyset$, $S_1 \cup S_2 = S$ and $\forall k \in \{1, 2\}, \forall p_i, p_j \in S_k, i \neq j, p_i$ is not adjacent to p_j . First, S_1 is used for embedding, and S_2 for prediction; then S_2 for embedding, S_1 for prediction. Each of S_1 and S_2 takes half of the capacity. While recovering, reversibility can be ensured by first getting S_2 according to S_1 , and then S_1 according to S_2 . One important thing is that the first two rows and columns and the last row and column in the cover image are not within our consideration. Since the process of twice embedding is similar, we only take the first layer embedding for illustration: we scan the blue pixels from left to right and from top to bottom yields $S_1 = \{x_1, x_2, \dots, x_N\}$, and for each pixel x_i , the prediction value \hat{x}_i obtained by using the rhombus predictor is calculated as follows:

$$\hat{x}_i = \lceil \frac{v_1 + v_2 + v_3 + v_4}{4} \rceil \quad (1)$$

where v_1, v_2, v_3, v_4 are the four neighboring yellow pixels of x_i , which is shown in Figure 3. Then the prediction-error e_i is calculated as:

$$e_i = x_i - \hat{x}_i \quad (2)$$

And PEH represented by $h(e)$ is generated by counting the frequency of prediction-errors as:

$$h(e) = \#\{1 \leq i \leq N : e_i = e\}, \forall e \in \{-255, \dots, 255\} \quad (3)$$

For embedding, C-PEE selects bins -1 and 0 as the expansion bins, and then modifies the prediction-error e_i as:

$$e'_i = \begin{cases} e_i - 1, & e_i < -1 \\ e_i - m, & e_i = -1 \\ e_i + m, & e_i = 0 \\ e_i + 1, & e_i > 0 \end{cases} \quad (4)$$

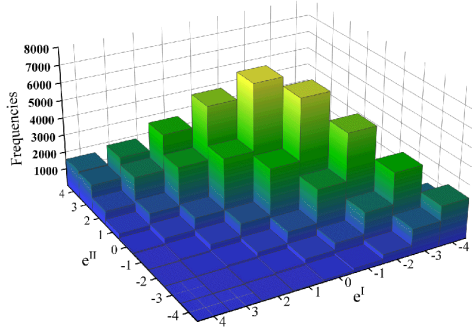
which means x_i is modified as follows:

$$x'_i = \begin{cases} x_i - 1, & e_i < -1 \\ x_i - m, & e_i = -1 \\ x_i + m, & e_i = 0 \\ x_i + 1, & e_i > 0 \end{cases} \quad (5)$$

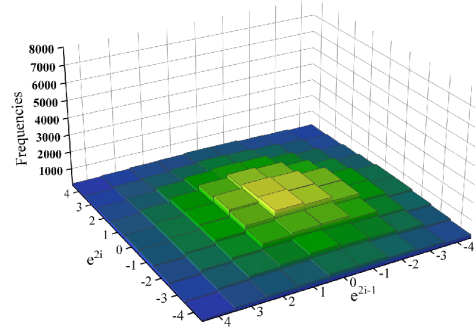
where $m \in \{0, 1\}$ is a to-be-embedded data, x'_i and e'_i are the modified pixel and prediction-error respectively. The modification of PEH during the embedding is shown in Figure 4: red arrows are expanded while green arrows are shifted.

As for extracting and recovering, reversibility is guaranteed by inverse scanning. For a marked pixel x'_i , we firstly calculate e'_i and recovery the original prediction-error e_i by e'_i as follows:

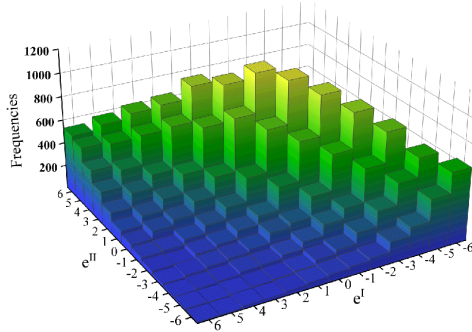
$$e_i = \begin{cases} e'_i, & e'_i \in \{-1, 0\} \\ e'_i + 1, & e'_i < -1 \\ e'_i - 1, & e'_i > 0 \end{cases} \quad (6)$$



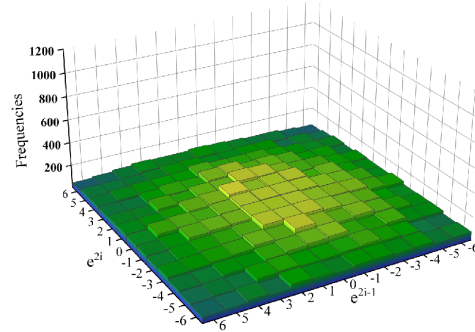
(a) 2D-PEH of image lena generated by our proposed method



(b) 2D-PEH of image lena generated by pairwise-PEE



(c) 2D-PEH of image Baboon generated by our proposed method



(d) 2D-PEH of image Baboon generated by pairwise-PEE

Fig. 1. 2D-PEH comparison between the proposed method and C-PEE

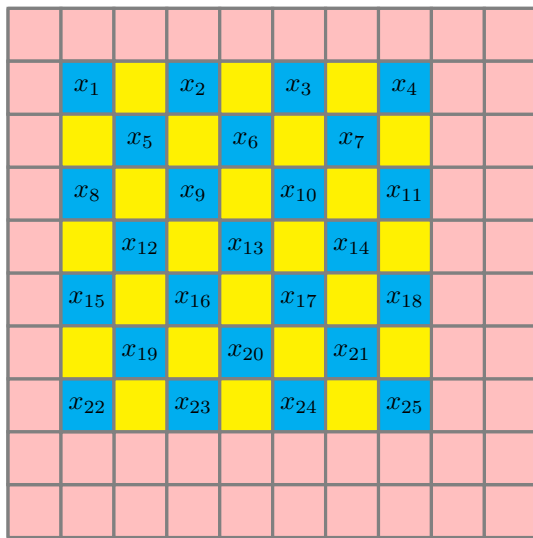


Fig. 2. partition of image pixels

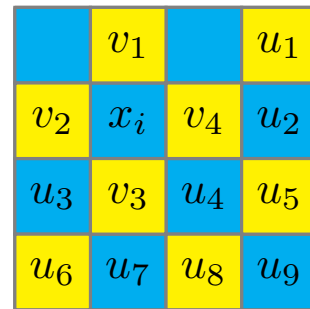


Fig. 3. prediction context of x_i

then recovery x_i as:

$$x_i = \begin{cases} x'_i, & e'_i \in \{-1, 0\} \\ x'_i + 1, & e'_i < -1 \\ x'_i - 1, & e'_i > 0 \end{cases} \quad (7)$$

where the secret message bit can be extracted as $m = 0$ when

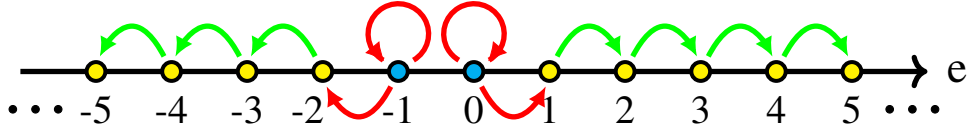


Fig. 4. mapping of C-PEE

$e_i \in \{-1, 0\}$, or $m = 1$ when $e_i \in \{-2, 1\}$.

B. MHM

As an extension of C-PEE, MHM divides pixels into distinct categories by measuring complexity, and adaptively selects expansion bins for each PEH. Specifically, for x_i , we take n_i as follows:

$$\begin{aligned}
 n_i = & |v_1 - \hat{x}_i| + |v_2 - \hat{x}_i| + |v_3 - \hat{x}_i| + |v_4 - \hat{x}_i| + \\
 & |u_3 - v_3| + |v_3 - u_4| + |u_4 - u_5| + |u_6 - u_7| + \\
 & |u_7 - u_8| + |u_8 - u_9| + |v_2 - u_3| + |u_3 - u_6| + \\
 & |v_3 - u_7| + |v_4 - u_4| + |u_4 - u_8| + |u_1 - u_2| + \\
 & |u_2 - u_5| + |u_5 - u_9| + |v_4 - u_2| \quad (8)
 \end{aligned}$$

where $\{v_1, v_2, v_3, v_4, u_1, u_2, \dots, u_9\}$ are the pixels in the context of x_i , which is shown in Figure 3. Then $M-1$ thresholds $\{s_0, s_1, \dots, s_{M-2}\}$ are determined based on the complexity n_i , the range of n_i is scaled to M values $\{V_0, V_1, \dots, V_{M-1}\}$, i.e., $V_0 = [0, s_0]$, $V_1 = [s_0 + 1, s_1]$, \dots , $V_{M-2} = [s_{M-3} + 1, s_{M-2}]$, $V_{M-1} = [s_{M-2} + 1, \infty)$.

Thresholds sequence is determined by computing the M -quantile of complexity n_i so that the number of pixels in each category is as uniform as possible, and the formal description of the thresholds calculation is as follows:

$$s_i = \arg \min_{th} \left\{ \frac{\#\{1 \leq j \leq N : n_j \leq th\}}{N} \geq \frac{i+1}{M} \right\} \quad (9)$$

Correspondingly, original PEH is split into $h_0(e), h_1(e), \dots, h_{M-1}(e)$ as well, where $h_t(e)$ denotes the frequency of prediction-errors with the local complexities belong to V_t :

$$h_t(e) = \#\{1 \leq i \leq N : e_i = e, n_i = t\} \quad (10)$$

Different from C-PEE, which selects fixed expansion bins of 0 and -1, MHM adaptively selects expansion bins for each PEH to reduce distortion. Specifically, the expansion bins are determined through the following optimization problem:

$$\begin{cases}
 \text{minimize} & \frac{\sum_{t=0}^{M-1} (\sum_{e < \text{bin}_a^t} h_t(e) + \sum_{e > \text{bin}_b^t} h_t(e))}{\sum_{t=0}^{M-1} h_t(\text{bin}_a^t) + h_t(\text{bin}_b^t)} \\
 \text{subject to} & \sum_{t=0}^{M-1} (h_t(\text{bin}_a^t) + h_t(\text{bin}_b^t)) \geq EC_{exp}
 \end{cases} \quad (11)$$

Here, $\text{bin}_{(t,a)}$ and $\text{bin}_{(t,b)}$ are the expansion bins selected for the t -th PEH, and EC_{exp} is the demand for embedding capacity. Figure 5 illustrates the modification mechanism

of multiple histograms in MHM, where $(\text{bin}_{0,a}, \text{bin}_{0,b}) = (-1, 1)$, $(\text{bin}_{1,a}, \text{bin}_{1,b}) = (-3, 1)$, $(\text{bin}_{2,a}, \text{bin}_{2,b}) = (-4, 4) \dots (\text{bin}_{t,a}, \text{bin}_{t,b}) = (-\infty, \infty), \forall t > 2$.

III. PROPOSED METHOD

In this section, we will describe our proposed method as follows: selection of distinct predictors, 2D-PEH based embedding, determination of optimal parameters and implementation details.

A. Selection of Distinct Predictors

We discuss C-PEE firstly, noting the number of pixels with prediction-error e_i as $h(e_i)$ and (a, b) as expansion bins, the embedding capacity and mean square error are:

$$EC = h(e_a) + h(e_b) \quad (12)$$

$$\begin{aligned}
 MSE &= \frac{1}{n \times m} \times \left(\sum_{e_i=-255}^{e_a} h(e_i) + \sum_{e_i=e_b}^{255} h(e_i) \right) \\
 &= 1 - \frac{1}{n \times m} \sum_{e_i=e_a}^{e_b} h(e_i) \quad (13)
 \end{aligned}$$

In general, we aim to maximize the embedding capacity EC while minimizing the mean square error MSE . Previous works have demonstrated that the higher the accuracy of the predictor, the smaller absolute value of the prediction-error will be, and PEH tends to follow a Laplace distribution, thus the distortion of the embedded image will be smaller. In summary, predictor accuracy is one of the main factors that determine the quality of the embedded image.

After conducting research, we found that all linear predictors, regardless of the accuracy, always perform better in predicting some of the same pixels but not for others. That is to say, most of the linear predictors predicted results with high correlation. However, for pixels with large prediction-errors which are predicted by linear predictors, the nonlinear ones may perform better, while for pixels which are predicted more accurately, the nonlinear ones may not perform well. Therefore, how to apply these two types of predictors to predict these pixels efficiently is of great importance to improve the quality of the embedded image, and we choose both of the linear one and the nonlinear one to calculate the prediction-error simultaneously.

Based on II-A, we modify the definition h to:

$$h(e^I, e^{II}) = \#\{-255 \leq e^I, e^{II} \leq 255 : e_i^I = e^I, e_i^{II} = e^{II}\} \quad (14)$$

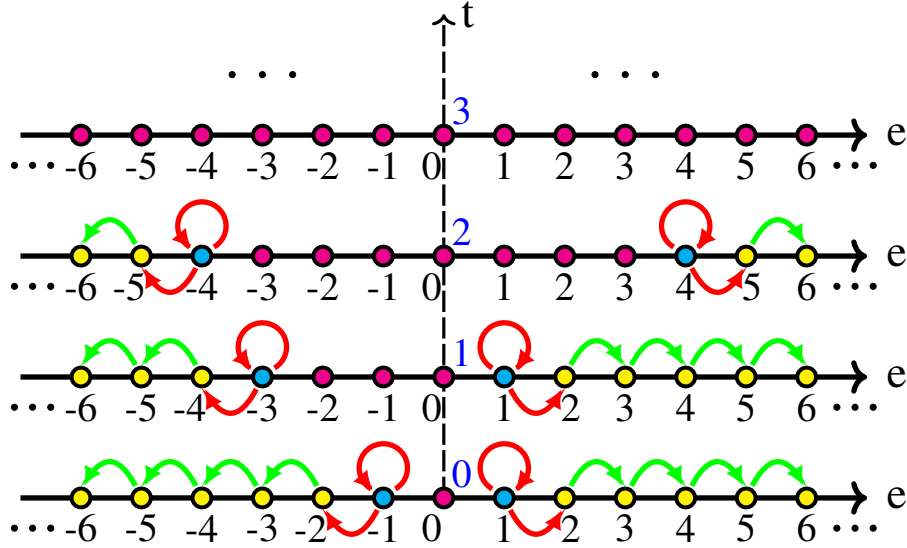


Fig. 5. mapping of MHM

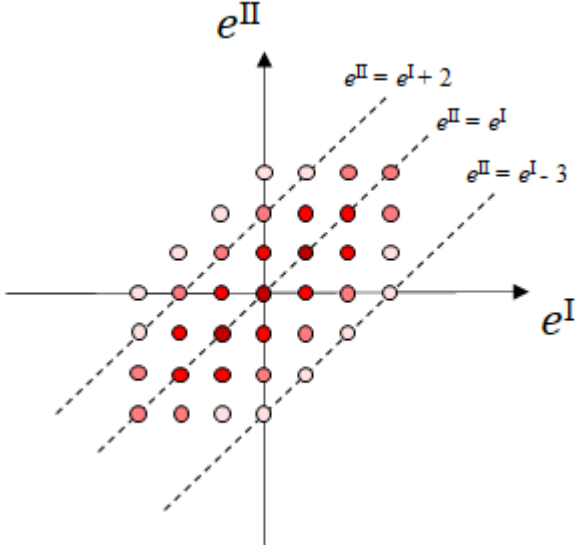


Fig. 6. color map of 2D-PEH

where e_i^I and e_i^{II} are prediction-errors derived by the two distinct predictors respectively. $h(e^I, e^{II})$ denotes the frequency of pixels whose double prediction-errors are e^I and e^{II} . As shown in figure 6, the darker the color, the larger the value of histogram $h(e^I, e^{II})$, so as to observe the distribution of $h(e^I, e^{II})$ clearly.

B. 2D-PEH Based Embedding

The 2D-PEH mentioned in III-A can be regarded as consisting of a number of 1D-PEHs, each of which can be mapped into the function image $e^{II} = e^I + b, b \in [-255, 255]$, i.e., the line corresponding to each b can be viewed as one 1D-PEH. Figure 6 labels the line $e^{II} = e^I + b$ when $b = -3, 0, 2$. Our target is to select a pair of expansion bins for each line

$e^{II} = e^I + b$ contained in the 2D-PEH. When reflected on Figure 6, that is, two points (p_b, q_b) and (r_b, s_b) have to be selected for each line $e^{II} = e^I + b$. It is required that the total distortion is minimized while ensuring that the expansion bins of the 1D-PEHs satisfy the embedding capacity requirement. We denote the embedding as EC and the distortion as ED , which can be calculated as follows:

$$EC = \sum_{b=-255}^{255} (h(p_b, q_b) + h(r_b, s_b)) \quad (15)$$

$$ED = \frac{1}{2}EC + \sum_{b=-255}^{255} \sum_{e_b^I < p_b \vee e_b^I > s_b} h(e_b^I, e_b^{II}) \quad (16)$$

Then, for x_i , modify its double prediction-errors (e_i^I, e_i^{II}) to be $(e_i^{I'}, e_i^{II'})$ based on (p_b, q_b) and (r_b, s_b) as:

$$(e_i^{I'}, e_i^{II'}) = \begin{cases} (e_i^I, e_i^{II}), & p_b < e_i^I < q_b \\ (e_i^I + m, e_i^{II} + m), & e_i^I = q_b \\ (e_i^I - m, e_i^{II} - m), & e_i^I = p_b \\ (e_i^I + 1, e_i^{II} + 1), & e_i^I > q_b \\ (e_i^I - 1, e_i^{II} - 1), & e_i^I < p_b \end{cases} \quad (17)$$

where $m \in \{0, 1\}$ is to-be-embedded data. Thereafter, x_i is modified to x_i' as follows:

$$x_i' = \begin{cases} x_i, & p_b < e_i^I < q_b \\ x_i + m, & e_i^I = q_b \\ x_i - m, & e_i^I = p_b \\ x_i + 1, & e_i^I > q_b \\ x_i - 1, & e_i^I < p_b \end{cases} \quad (18)$$

For greater clarity, we show this process in Figure 7.

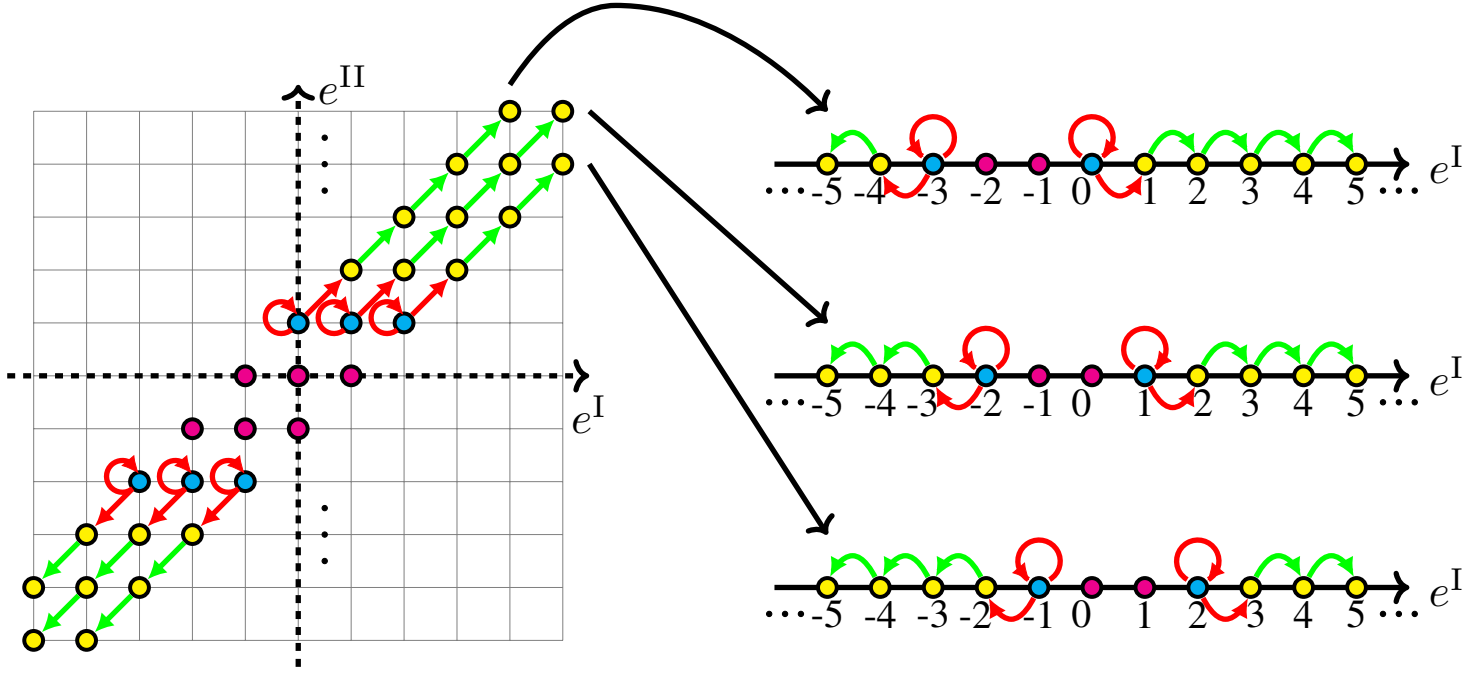


Fig. 7. example of 2D-PEH modification

Due to the use of distinct predictors for prediction, we can classify the pixels in a more detailed way. Therefore, there are more optional expansion bins when embedding, which helps us to increase the capacity and reduce the distortion. To better demonstrate the performance of our proposed method, a comparison of the experimental result with C-PEE on Lena and Baboon is shown in Figure 8, in which C-PEE uses rhombus predictor, double-layered embedding. Our proposed method uses rhombus predictor and MED, double-layered embedding as well. Specifically, \hat{x}_i^I is computed as:

$$\hat{x}_i^I = \lceil \frac{v_1 + v_2 + v_3 + v_4}{4} \rceil, \quad (19)$$

and \hat{x}_i^{II} is calculated as:

$$\hat{x}_i^{II} = \begin{cases} \min(v_3, v_4), & u_4 \geq \max(v_3, v_4) \\ \max(v_3, v_4), & u_4 \leq \min(v_3, v_4) \\ v_3 + v_4 - u_4, & \text{otherwise.} \end{cases} \quad (20)$$

The double prediction-errors (e_i^I, e_i^{II}) is calculated as:

$$(e_i^I, e_i^{II}) = (x_i - \hat{x}_i^I, x_i - \hat{x}_i^{II}) \quad (21)$$

Then, we generate 2D-DPEH as illustrated in III-A and embed secret message according to (17) and (18). The results in Figure 8 has shown that our proposed 2D-DPEH Embedding has a significant improvement in PSNR compared to C-PEE, which is 2.35dB higher on average. The experiments verify the feasibility of the distinct predictors and the superiority of the proposed method.

Next, we extend the proposed method to multiple 2D-DPEHs by combining it with MHM to further verify the theoretical value of it. The flowchart of the method is shown as 9. We first calculate the complexity n_i and double prediction-errors e_i^I, e_i^{II} of each pixel x_i . Since previous works have demonstrated that the full-enclosing-based predictor performs better than half-enclosing-based predictor in accuracy, the implementation of multiple 2D-PEHs employs two distinct rhombus predictors. For the linear rhombus prediction, we utilize the mean prediction, i.e., \hat{x}_i^I computed by (18). As for the nonlinear rhombus prediction, we design it based on MED [6], which first calculates the vertical and horizontal intensities I_1 and I_2 of the image edges separately:

$$\begin{cases} I_1 = \frac{1}{n \times m} \sum_{i=0}^{n-1} \sum_{j=0}^{m-1} (x_{i-1,j+1} + x_{i,j+1} + x_{i+1,j+1} \\ \quad \quad \quad - x_{i-1,j-1} - x_{i,j-1} - x_{i+1,j-1}) \\ I_2 = \frac{1}{n \times m} \sum_{i=0}^{n-1} \sum_{j=0}^{m-1} (x_{i-1,j-1} + x_{i-1,j} + x_{i-1,j+1} \\ \quad \quad \quad - x_{i+1,j-1} - x_{i+1,j} - x_{i+1,j+1}) \end{cases} \quad (22)$$

The prediction-error \hat{x}_i^{III} is calculated as follows:

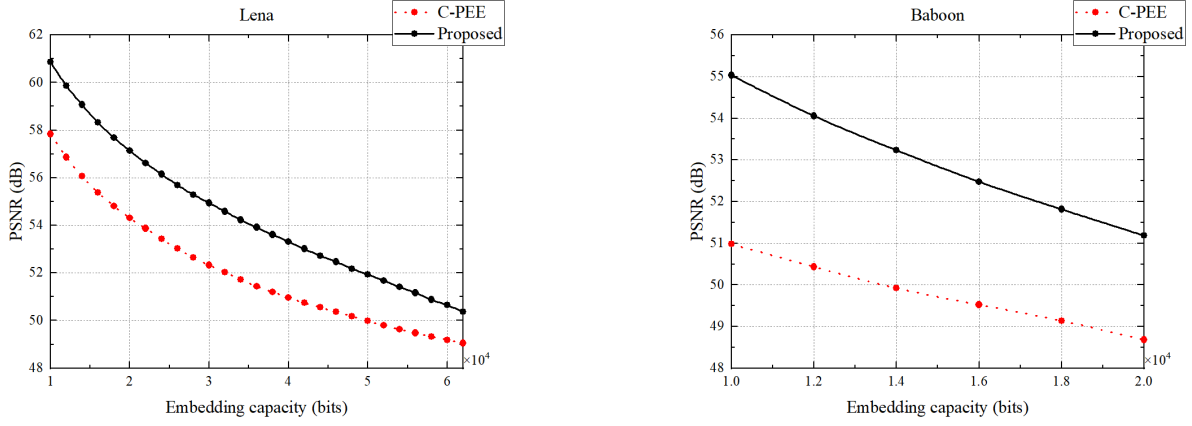


Fig. 8. Performance comparison between the proposed method and C-PEE

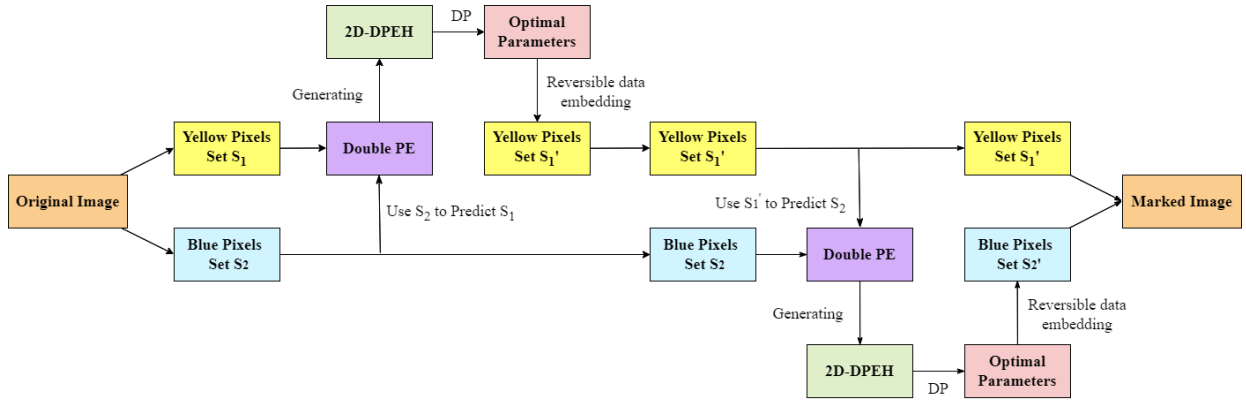


Fig. 9. The flow chart of proposed method

$$\hat{x}_i^{\text{II}} = \begin{cases} \lceil \frac{\max(v_1, v_2) + \min(v_3, v_4)}{2} \rceil, \min(v_1, v_2) \geq \max(v_3, v_4) \\ \lceil \frac{\max(v_2, v_3) + \min(v_1, v_4)}{2} \rceil, \min(v_2, v_3) \geq \max(v_1, v_4) \\ \lceil \frac{\max(v_3, v_4) + \min(v_1, v_2)}{2} \rceil, \min(v_3, v_4) \geq \max(v_1, v_2) \\ \lceil \frac{\max(v_1, v_4) + \min(v_2, v_3)}{2} \rceil, \min(v_1, v_4) \geq \max(v_2, v_3) \\ \lceil \frac{v_1 + v_3}{2} \rceil, \min(v_1, v_3) \geq \max(v_2, v_4), I_1 \geq I_2 \\ \lceil \frac{v_2 + v_4}{2} \rceil, \min(v_2, v_4) \geq \max(v_1, v_3), I_1 < I_2 \end{cases} \quad (23)$$

The 2D-DPEH generated by our proposed method is shown in Figure 1 (a) (c). Then the double prediction-errors e_i^{I} and e_i^{II} are calculated as follows:

$$\begin{cases} e_i^{\text{I}} = x_i - \hat{x}_i^{\text{I}} \\ e_i^{\text{II}} = x_i - \hat{x}_i^{\text{II}} \end{cases} \quad (24)$$

After that, $M - 1$ thresholds are determined based on n_i , which divide the thresholds sequence into M intervals $V_0 = [0, s_0], V_1 = [s_0 + 1, s_1], \dots, V_{M-2} = [s_{M-3} +$

$1, s_{M-2}], V_{M-1} = [s_{M-2} + 1, \infty)$, and M 2D-DPEHs are generated accordingly. Thus the prediction-errors are uniformly partitioned into M 2D-DPEHs:

$$h_t(e^{\text{I}}, e^{\text{II}}) = \#\{-255 \leq e^{\text{I}}, e^{\text{II}} \leq 255 : e_i^{\text{I}} = e^{\text{I}}, e_i^{\text{II}} = e^{\text{II}}, n_i \in V_t\} \quad (25)$$

At this time, our target is to select a pair of expansion bins for each line $e^{\text{II}} = e^{\text{I}} + b$ contained in every 2D-DPEH, where the selected expansion bins of line $e^{\text{II}} = e^{\text{I}} + b$ belonging to the t -th histogram are equivalent to the points $(p_{t,b}, q_{t,b})$ and $(r_{t,b}, s_{t,b})$ on the Figure 10. The total distortion is required to be minimized while ensuring that the expansion bins of the 1D-PEHs corresponding to these points satisfy the capacity demand. The equations for EC and ED are thus modified as follows:

$$EC = \sum_{t=0}^{M-1} \left(\sum_{b=-255}^{255} (h(p_{t,b}, q_{t,b}) + h(r_{t,b}, s_{t,b})) \right) \quad (26)$$

$$ED = \frac{1}{2}EC + \sum_{t=0}^{M-1} \left(\sum_{b=-255}^{255} \left(\sum_{\substack{e_{t,b}^{\text{I}} < p_{t,b} \\ e_{t,b}^{\text{II}} > s_{t,b}}} h(e_{t,b}^{\text{I}}, e_{t,b}^{\text{II}}) \right) \right) \quad (27)$$

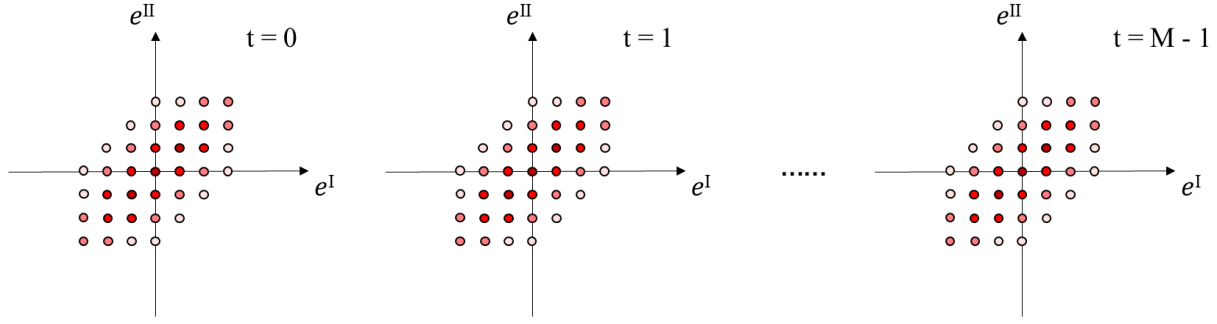


Fig. 10. Example of multiple 2D-PEH

Similarly, (e_i^I, e_i^{II}) and x_i are recalculated as follows:

$$(e_i^{I'}, e_i^{II'}) = \begin{cases} (e_i^I, e_i^{II}), & p_{t,b} < e_i^I < q_{t,b} \\ (e_i^I + m, e_i^{II} + m), & e_i^I = q_{t,b} \\ (e_i^I - m, e_i^{II} - m), & e_i^I = p_{t,b} \\ (e_i^I + 1, e_i^{II} + 1), & e_i^I > q_{t,b} \\ (e_i^I - 1, e_i^{II} - 1), & e_i^I < p_{t,b} \end{cases} \quad n_i \in V_t \quad (28)$$

$$x_i' = \begin{cases} x_i, & p_{t,b} < e_i^I < q_{t,b} \\ x_i + m, & e_i^I = q_{t,b} \\ x_i - m, & e_i^I = p_{t,b} \\ x_i + 1, & e_i^I > q_{t,b} \\ x_i - 1, & e_i^I < p_{t,b} \end{cases} \quad n_i \in V_t \quad (29)$$

More specifically, when the value of x_i changes by 1, the double prediction-errors e_i^I and e_i^{II} also change by 1 at the same time, which is reflected in a shift from (e_i^I, e_i^{II}) to $(e_i^I \pm 1, e_i^{II} \pm 1)$ in the 2D-DPEH. Therefore, we can describe this by the following linear function:

$$e_i^{II} = e_i^I + b, \quad \forall b \in [-255, 255] \quad (30)$$

When we employ only one predictor, all pixels with equal prediction-error have the same decision. Therefore, when the case is two distinct predictors, to ensure consistency before and after decision-making, it is necessary to group all points satisfying $e^{II} = e^I + b$ into one category and discuss separately. Moreover, when the two predictors are the same, all points on the 2D-DPEH are clustered on the line $e^{II} = e^I$. In this case, multiple 2D-PEHs are equivalent to *MHM*, in other words, *MHM* can be regarded as a subset of multiple 2D-DPEHs. Therefore, our proposed method must not be inferior to *MHM*.

Similarly, for multiple 2D-PEHs secret message extraction and image recovery, we first calculate the complexity n_i of the currently modified pixel \hat{x}_i , and trace to its corresponding 2D-DPEH h_t based on the thresholds sequence. Then we can get b by following (30) to find the corresponding 1D-PEH in h_t and

the expansion bins $(p_{t,b}, q_{t,b})$. The original double prediction-errors can be calculated based on $(e_i^{I'}, e_i^{II'})$ and $(p_{t,b}, q_{t,b})$ as follows:

$$(e_i^I, e_i^{II}) = \begin{cases} (e_i^{I'}, e_i^{II'}) & p_{t,b} \leq e_i^{I'} \leq q_{t,b} \\ (e_i^{I'} - 1, e_i^{II'} - 1) & e_i^{I'} > q_{t,b} \\ (e_i^{I'} + 1, e_i^{II'} + 1) & e_i^{I'} < p_{t,b} \end{cases} \quad n_i \in V_t \quad (31)$$

Then, we recover the current pixel as $x_i = \hat{x}_i + e_i^I$. In addition, when $e_i^{I'} \in \{p_{t,b}, q_{t,b}\}$, the embedded data is 0, and when $e_i^{I'} \in \{p_{t,b} - 1, q_{t,b} + 1\}$, the embedded one is 1.

C. Determination of Optimal Parameters

As mentioned above, for each 1D-PEH in the 2D-PEH, we need to select a pair of expansion bins, which is reflected in Figure 6, i.e., selecting two points with coordinates $(p_{t,b}, q_{t,b})$ and $(r_{t,b}, s_{t,b})$ respectively. The selection is based on minimizing distortion under the requirement of capacity, which involves solving the following constrained optimization problem:

$$\begin{cases} ED = \sum_{t=0}^{M-1} \sum_{b=-255}^{255} \left(\sum_{e < p_{t,b}} h_t(e, e+b) + \sum_{e > q_{t,b}} h_t(e, e+b) \right) \\ EC = \sum_{t=0}^{M-1} \sum_{b=-255}^{255} h_t(p_{t,b}, p_{t,b} + b) + h_t(q_{t,b}, q_{t,b} + b) \\ \text{minimize } \frac{ED}{EC} \\ \text{subject to } EC \geq EC_{exp} \end{cases} \quad (32)$$

Considering the embedding capacity that most 1D-PEHs can provide is not even sufficient for the bits of auxiliary information needed to record their parameters, lines $e^{II} = e^I + b$ that correspond to bin heights of 1D-PEHs with a sum of less than H will be categorized as invalid lines which will not be taken into account by us. Here, H is empirically taken as 20.

Furthermore, in *MHM*, parameters are determined by exhaustive search and the time cost is reduced by setting constraints. However, for our proposed algorithm, the time complexity of the exhaustive search is unacceptable, while too many constraints will degrade the quality of the embedded

image. Therefore, we utilize DP to solve this problem and optimize the time complexity while achieving better results. In the following part, we will introduce **Optional Expansion Bins Processing** and **DP For Optimal Expansion Bins** specifically.

1) *Optional Expansion Bins Processing*: We first preprocess $EC_{t,b}^k$ and $ED_{t,b}^k$ for all the optional expansion bins of 1D-PEH corresponding to the lines in each 2D-PEH, i.e., $EC_{t,b}^k$ and $ED_{t,b}^k$ denote the capacity and distortion by selecting the k -th optional expansion bins of $e^{\text{II}} = e^{\text{I}} + b$ in t -th 2D-PEH, respectively. However, in II, we have shown that 1D-PEH generated by using the linear rhombus predictor will be much sharper, so that ultimately most of the selections of expansion bins will be relatively concentrated in a small range. Thus there is no need to process out all the optional expansion bins for each line $e^{\text{II}} = e^{\text{I}} + b$, which optimizes the time cost and reduces the amount of auxiliary information. Only bins of $x \in [-14, 14]$ are taken into account.

Specifically, we traverse points of $e_i^{\text{I}} \in [-14, 14]$ on each valid line $e^{\text{II}} = e^{\text{I}} + b$ for every 2D-DPEH, which will produce the following three possible options shown in Figure ??.

- Take $(e_i^{\text{I}}, e_i^{\text{II}})$ as expansion bin a, (∞, ∞) as expansion bin b, EC is $h_t(e_i^{\text{I}}, e_i^{\text{II}})$, ED is $\frac{1}{2}h_t(e_i^{\text{I}}, e_i^{\text{II}}) + \sum_{e_j^{\text{I}} < e_i^{\text{I}}} h_t(e_j^{\text{I}}, e_j^{\text{II}})$
- Take $(-\infty, -\infty)$ as expansion bin a, $(e_i^{\text{I}}, e_i^{\text{II}})$ as expansion bin b, EC is $h_t(x_i, y_i)$, ED is $\frac{1}{2}h_t(e_i^{\text{I}}, e_i^{\text{II}}) + \sum_{e_j^{\text{I}} > e_i^{\text{I}}} h_t(e_j^{\text{I}}, e_j^{\text{II}})$
- Take $(e_i^{\text{I}}, e_i^{\text{II}})$ as expansion bin a, $(e_j^{\text{I}}, e_j^{\text{II}})$ as expansion bin b, $x_i < x_j$, EC is $h_t(x_i, y_i) + h_t(x_j, y_j)$, ED is $\frac{1}{2}(h_t(e_i^{\text{I}}, e_i^{\text{II}}) + h_t(e_j^{\text{I}}, e_j^{\text{II}})) + \sum_{e_k^{\text{I}} < e_i^{\text{I}}} h_t(e_k^{\text{I}}, e_k^{\text{II}}) + \sum_{e_l^{\text{I}} > e_j^{\text{I}}} h_t(e_l^{\text{I}}, e_l^{\text{II}})$

For example, now on the line $y = x + 3$ of 2D-DPEH whose complexity belongs to V_2 , the points $(e^{\text{I}}, e^{\text{II}})$ of $h_2(e^{\text{I}}, e^{\text{II}}) > 0$ include $\{(-16, -13), (0, 3), (1, 4), (5, 8), (12, 15)\}$: $h_2(-16, -13) = 150, h_2(0, 3) = 100, h_2(1, 4) = 300, h_2(5, 8) = 200, h_2(12, 15) = 250$.

Due to $-16 < -14$, point $(-16, -13)$ is beyond the search range, which is not taken into consideration. Assuming we are currently processing $(1, 4)$, as mentioned above, the following cases are possible:

- Take $(1, 4)$ as expansion bin a, (∞, ∞) as expansion bin b, EC is $h_2(1, 4) = 300$, ED is $\frac{1}{2}h_2(1, 4) + h_2(-16, -13) + h_2(0, 3) = 400$
- Take $(-\infty, -\infty)$ as expansion bin a, $(1, 4)$ as expansion bin b, EC is $h_2(1, 4) = 300$, ED is $\frac{1}{2}h_2(1, 4) + h_2(5, 8) + h_2(12, 15) = 600$
- Take $(1, 4)$ as expansion bin a, $(5, 8)$ as expansion bin b, EC is $h_2(1, 4) + h_2(5, 8) = 500$, ED is $\frac{1}{2}(h_2(1, 4) + h_2(5, 8)) + h_2(-16, -13) + h_2(0, 3) + h_2(12, 15) = 750$
- Take $(1, 4)$ as expansion bin a, $(12, 15)$ as expansion bin b, EC is $h_2(1, 4) + h_2(12, 15) = 550$, ED is $\frac{1}{2}(h_2(1, 4) + h_2(12, 15)) + h_2(-16, -13) + h_2(0, 3) = 525$

For $(0, 3), (5, 8), (12, 15)$, similarly, we add the above cases to the decision-making alternatives of this group for the

upcoming DP.

2) *DP For Optimal Expansion Bins*: To delineate more clearly, the parameters of DP For Optimal Expansion Bins are defined using the symbols shown in Table I.

We first design the state and boundary conditions, and let $f_{t,i,j}$ denote the minimum distortion caused by the first t 2D-DPEHs, the t -th one only consider lines with $-255 \sim i$ intercepts, and based on the condition of the embedding capacity requirement is j . Since the sum of the capacity provided by the expansion bins is allowed to exceed EC_{exp} , the maximum value j of the DP array $f_{t,i,j}$ is taken as $EC_{exp} + \Delta$ in the design of the state boundary, where Δ is a increment to prevent the sum from being out-of-bounds, Δ is taken as 2,000 based on several experiments. Obviously, if no expansion bins are selected, the total EC and ED are both 0, so the boundary condition is as follows:

$$f_{-1,255,j} = \begin{cases} 0, & j = 0 \\ \infty, & j \neq 0 \end{cases} \quad (33)$$

Then the state-transition equation is designed as follows:

$$f_{t,i,j} = \begin{cases} \min_k(f_{t,i-1,j}, f_{t,i-1,j-EC_{t,i,k}} + ED_{t,i,k}), & i > -255 \\ \min_k(f_{t-1,255,j}, f_{t-1,255,j-EC_{t,i,k}} + ED_{t,i,k}), & i = -255 \end{cases} \quad (34)$$

Based on the boundary conditions 33, iterate continuously according to the state-transition equation 34, and end up getting $f_{M-1,255,j}$, which denotes the minimum distortion under the condition that the embedding capacity requirement is j , the specific process of forward state-transition is shown as Algorithm 1.

Eventually, we will backtrack to obtain the optimal parameters, in addition to determining the minimum distortion, the exact indexes of selected expansion bins for embedding are desired as well. So it is necessary to record the transfer paths during the DP process, let $trans_{t,i,j}$ denote the transfer source of $f_{t,i,j}$:

$$trans_{t,i,j} = \begin{cases} \underset{k}{\operatorname{argmin}}\{f_{t,i-1,j-EC_{t,i,k}} + ED_{t,i,k}\}, & i > -255 \\ \underset{k}{\operatorname{argmin}}\{f_{t-1,255,j-EC_{t,i,k}} + ED_{t,i,k}\}, & i = -255 \end{cases} \quad (35)$$

Once the DP is finished, we determine the optimal embedding capacity (the one that satisfies the capacity requirements and minimizes distortion) that the expansion bins are able to offer by the following equation, denoted as EC^* :

$$EC^* = \underset{j \geq EC_{exp}}{\operatorname{argmin}}\{f_{M-1,255,j}\} \quad (36)$$

Then we obtain the above-mentioned indexes by reverse-traversing the array $trans$, the details are shown in Algorithm 2.

Considering that DP needs a huge space to store the state information, we decide to optimize the space complexity by scrolling array. DP topic is a bottom-up expansion technique,

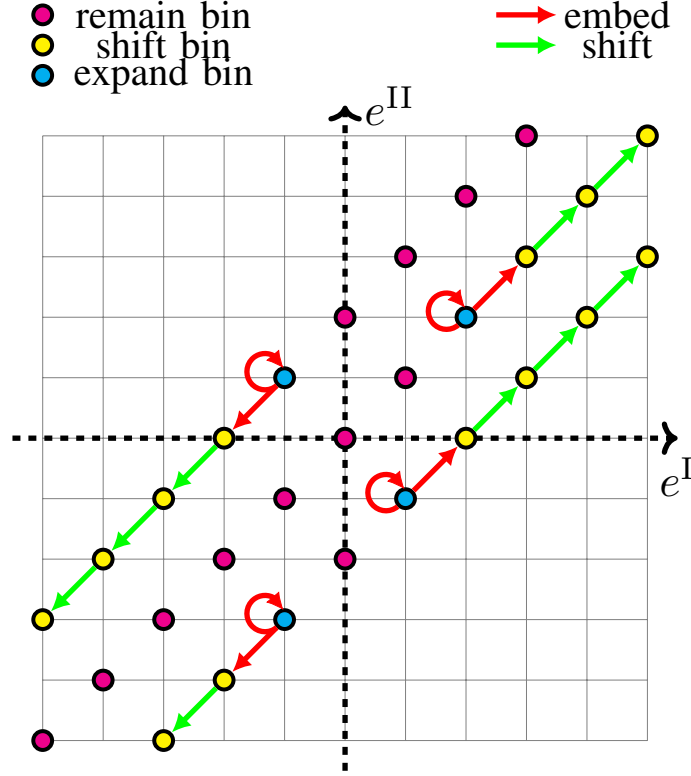


Fig. 11. item illustration

TABLE I
DEFINITION OF SYMBOLS IN DP

symbol	definition
$f_{t,i,j}$	the minimum distortion caused by the first t 2D-PEHs, the t -th one considers the lines with intercepts of $-255 \sim i$, while satisfying the embedding capacity requirement of j .
$trans_{t,i,j}$	the transfer source of $f_{t,i,j}$
$exBin_{t,i,k}$	the k -th optional expansion bins of a line with intercept i in the t -th 2D-DPEH.
$EC_{t,i,k}$	the embedding capacity offered by $exBin_{t,i,k}$.
$ED_{t,i,k}$	the distortion caused by $exBin_{t,i,k}$.
$n_{t,i}$	the number of optimal expansion of the line with intercept i in the t -th 2D-DPEH.
$optBin_{t,i}$	the optimal expansion of a line with intercept i in the t -th 2D-DPEH.
Δ	a increment to prevent the array out of bounds.

according to (34), we find that $f_{t,i,j}$ is transferred from only $f_{t,i-1,k}$ or $f_{t-1,255,k}$. In other words, the state information stored more previously is useless for $f_{t,i,j}$, which means that some parts of the stored state information can be shed as DP progresses. More specifically, we redefine the states f_j, g_j as follows:

$$\begin{cases} g_j = \min\{f_j, \min_k\{f_{j-EC_{t,i,k}} + ED_{t,i,k}\}\} \\ f_j = g_j \end{cases} \quad (37)$$

where f_j and g_j represent the dp result of the last group and the dp result of the current one, j denotes the size of the capacity and k denotes the k -th pair of optional expansion bins that is being processed in the current group. The meaning of Equation (37) is that g_j is obtained by transforming from f_j first, and then g_j is assigned to f_j to prepare for the transfer of the next round, the process will continue until getting all

of the optimal expansion bins. It can be shown that the space complexity of the proposed method is reduced from the initial $O(M \times 511 \times EC_{exp})$ to $O(EC_{exp})$ (EC_{exp} denotes the expected embedding capacity), thus saving a lot of space.

Now assume that the b -th line in the t -th 2D-DPEH contains $c_{t,b}$ pairs of optional expansion bins. Compared to the exhaustive search, DP optimizes the time cost from $\prod_{t=0}^{M-1} \prod_{b=-255}^{255} c_{t,b}$ to $\sum_{t=0}^{M-1} \sum_{b=-255}^{255} c_{t,b} \times EC$. In short, the time complexity is now optimized by us from exponential to polynomial level. When in the embedding capacities of 10,000 bits on image Lena, the exhaustive search theoretically takes more than $10^{7000} s$, but the experimental results show that the proposed method optimized by DP only takes about 30s on C++, which definitely proves the effectiveness of DP.

E. Data Extraction and Image Restoration

Still taking the first layer of embedding as an example, at the beginning, we obtain S_{aux} by taking LSB of the first 10 pixels in the last row, and then we take LSB of 11 to S_{aux} pixels and decompress them to determine the auxiliary information. After that, the S_{LSB} of $(x_{N'+1}, \dots, x_{N_{end}})$ is extracted and restored by scanning in reverse order based on above-mentioned method, and we realize restoration for the last row by replacing LSBs of first S_{aux} pixels with extracted S_{LSB} . Finally, also in reverse scanning order, extract the embedded secret message from $(x_1, \dots, x_{N'})$ and meanwhile restore these pixels according to III. It is important to note that for each overflow or underflow pixel x_i recorded in CLM , modify its value to 255 if $x_i = 254$, or 0 if $x_i = 1$.

From Figure 13, even though the embedded image quality has achieved a very high level of performance by adopting MHM, the proposed method still improves MHM with an average PSNR gain of 0.50dB and 1.65dB, respectively. The experiment results prove the feasibility of extending 2D-DPEH to multiple 2D-DPEHs and the superiority of the proposed method.

IV. EXPERIMENTAL RESULTS

In this section, we mainly evaluate the performance of the proposed method by comparing it method with C-PEE, Pairwise PEE, original MHM, and several state-of-the-art works based on MHM, all of which adopt rhombus predictor, double-layered embedding. The M of MHM methods are taken as 16. Six standard 512×512 sized gray-scale images including Lena, Baboon, Barbara, Boat, Airplane and Peppers downloaded from the USC-SIPI image database are selected for experiments. At the same time, experimental results and parameters of 10,000 and 20,000 capacity are listed in the Table IV. Owing to space constraints, we only list the parameters $(p_{t,b}, r_{t,b})$ when $(0 \leq t \leq 2, -2 \leq b \leq 2)$. Here, $(p_{t,b}, r_{t,b})$ has the same meaning as in III.

For C-PEE, a very sharp 1D-PEH can be generated by rhombus predictor, double-layered embedding, has already achieved a good performance. However, from II and III, we can find that the average PSNR of the proposed method gains are 4.88 dB and 4.56 dB higher than C-PEE's in the embedding capacity of 10,000 and 20,000. For pairwise PEE proposed by Bo Ou et al., the capability of embedding is further improved by extending PEH to 2D and adaptively discarding the mapping direction with large distortion. From II and III, the proposed method outperforms pairwise PEE with an average PSNR increase of 2.33 dB and 2.10 dB in the embedding capacity of 10,000 bits and 20,000 bits respectively.

For original MHM proposed by Li Xiaolong et al., it initiatively proposes to generate series 1D-PEHs according to complexity thresholds, and select a pair of expansion bins in each PEH for embedding. From 14, we can see that MHM achieves good results on all kinds of images, and when the embedding capacity is 10,000 and 20,000, the average PSNR reaches a very high level: 60.04dB and 55.91dB respectively. However, from II and III, the performance of the proposed

method is still better than original MHM, improves it with an average PSNR gain of 0.95 dB and 0.96 dB. Since then, more and more researchers have conducted works based on MHM. Among them, the state-of-the-art works include High capacity MHM proposed by Bo Ou et al., in 2020, Optimal MHM proposed by Wenfa Qi et al., in 2020, and HMM-PRE proposed by Xiao Mengyao et al., in 2023. Unlike MHM, which selects only one pair of expansion bins, High capacity MHM selects multiple pairs of expansion bins for each PEH. Compared with other MHM-type algorithms, High capacity MHM not only achieves higher total embedding capacity, but also has a slower rate of performance degradation as the capacity increases. Optimal MHM optimizes MHM by continually continuously reducing the original problem to smaller subproblems. MHM-PRE replaces prediction-error with pixel-residual to establish multiple PRHs, and derives more expansion bins through a new mapping mechanism. From 14, although High capacity MHM, Optimal MHM and MHM-PRE perform well in these images, and both offer significant improvements over original MHM, the proposed method still outperforms them. It improves High capacity MHM with an average PSNR gain of 0.95 dB and 0.75 dB, improves Optimal MHM with an average PSNR gain of 0.79 dB and 0.76 dB, and improves MHM-PRE by 0.49 dB 与 0.54 dB PSNR gain in the embedding capacities of 10,000 bits and 20,000 bits, respectively. Moreover, on high-complexity image such as Baboon, the gain from double predictors will be more obvious, and the performance of the proposed method may perform even better.

To sum up, through comparison with C-PEE, Pairwise PEE, original MHM and several state-of-the-art methods based on MHM, the superiority and theoretical value of the proposed method is experimentally verified.

V. CONCLUSION

In this paper, we propose a improved 2D-PEH based on double prediction-error. First, different from previous 2D-PEH, the proposed 2D-DPEH is established by selecting two distinct predictors with low correlation to calculate double prediction-errors for each pixel. In addition, we adopt DP to optimize the selection of expansion bins, speeding up the running time and improving the quality of the embedded image. Finally, we combined the proposed method with C-PEE and original MHM, then designed comparative experiments with state-of-the-art PEE-based methods in recent years to verify the superiority of the proposed algorithm and extend PEE into a more general case.

REFERENCES

- [1] Bo Ou and Yao Zhao. 2020. High capacity reversible data hiding based on multiple histograms modification. *IEEE Transactions on Circuits and Systems for Video Technology* 30, 8 (2020), 2329–2342.
- [2] W. Qi, X. Li, T. Zhang, and Z. Guo. 2020. Optimal reversible data hiding scheme based on multiple histograms modification. *IEEE Transactions on Circuits and Systems for Video Technology* 30, 8 (2020), 2300–2312.
- [3] Xiaolong Li, Weiming Zhang, Xinlu Gui, and Bin Yang. 2015. Efficient reversible data hiding based on multiple histograms modification. *IEEE Transactions on Information Forensics and Security* 10, 9 (2015), 2016–2027.

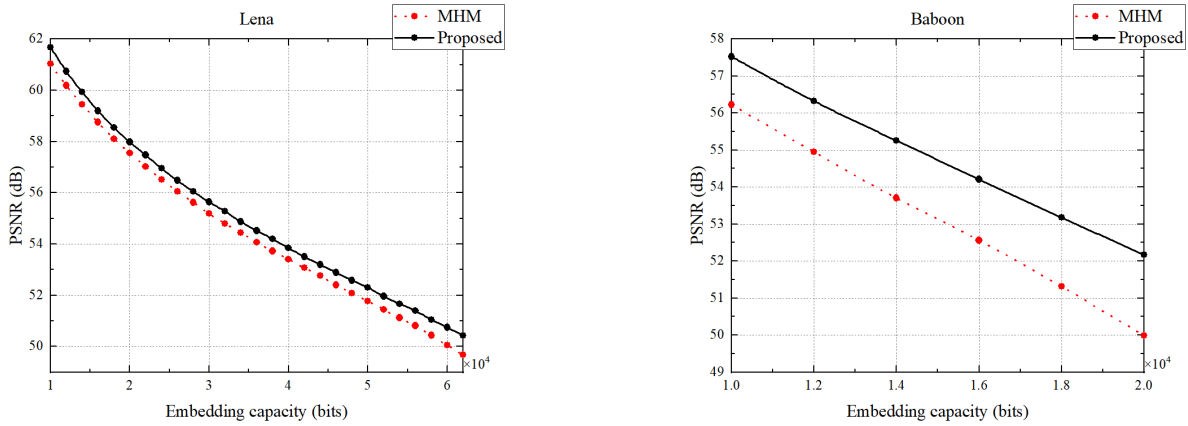


Fig. 13. Performance comparison between the proposed method and MHM

TABLE II

COMPARISON OF PSNR (IN DB) BETWEEN THE PROPOSED METHOD AND THE ORIGINAL MHM [X], MHM-PRE [Y], IN AN EMBEDDING CAPACITY OF 10,000 BITS

image	C-PEE	Pairwise PEE	MHM	High capacity MHM	Optimal MHM	MHM-PRE	Proposed
Lena	57.84	59.75	61.03	61.01	61.04	61.33	61.68
Baboon	50.98	55.21	56.22	56.23	56.25	56.90	57.52
Barbara	55.98	59.48	61.41	61.36	61.67	61.83	62.10
Boat	53.98	57.55	58.62	58.65	58.97	59.10	60.16
Airplane	63.9	63.76	63.87	63.89	63.90	64.26	64.25
Peppers	53.99	56.21	59.06	59.07	59.37	59.60	60.22
Average	56.11	58.66	60.04	60.04	60.20	60.50	60.99

TABLE III

COMPARISON OF PSNR (IN DB) BETWEEN THE PROPOSED METHOD AND THE ORIGINAL MHM [X], MHM-PRE [Y], IN AN EMBEDDING CAPACITY OF 20,000 BITS

image	C-PEE	Pairwise PEE	MHM	High capacity MHM	Optimal MHM	MHM-PRE	Proposed
Lena	54.31	56.21	57.56	57.55	57.64	57.79	57.98
Baboon	48.68	49.89	49.99	50.96	50.41	50.89	52.17
Barbara	53.52	56.22	57.67	57.68	57.79	57.96	58.25
Boat	50.74	53.32	54.58	54.76	54.85	55.03	55.96
Airplane	55.85	60.15	60.55	60.49	60.60	60.75	60.75
Peppers	50.74	52.83	55.12	55.25	55.37	55.55	56.12
Average	52.31	54.77	55.91	56.12	56.11	56.33	56.87

- [4] D. M. Thodi and J. J. Rodriguez, "Expansion embedding techniques for reversible watermarking," *IEEE Trans. Image Process.*, vol. 16, no. 3, pp. 721–730, Mar. 2007.
- [5] M. Fallahpour, "Reversible image data hiding based on gradient adjusted prediction," *IEICE Electron. Exp.*, vol. 5, no. 20, pp. 870–876, Oct. 2008.
- [6] Y. Hu, H.-K. Lee, and J. Li, "DE-based reversible data hiding with improved overflow location map," *IEEE Trans. Circuits Syst. Video Technol.*, vol. 19, no. 2, pp. 250–260, Feb. 2009.
- [7] W. Hong, T.-S. Chen, and C.-W. Shiu, "Reversible data hiding for high quality images using modification of prediction errors," *J. Syst. Softw.*, vol. 82, no. 11, pp. 1833–1842, Nov. 2009.
- [8] C. W. Honsinger, P. W. Jones, M. Rabbani, and J. C. Stoffel, "Lossless recovery of an original image containing embedded data," U.S. Patent 6 278 791, Aug. 21, 2001.
- [9] G. Coatrieux, C. Le Guillou, J.-M. Cauvin, and C. Roux, "Reversible watermarking for knowledge digest embedding and reliability control in medical images," *IEEE Trans. Inf. Technol. Biomed.*, vol. 13, no. 2, pp. 158–165, Mar. 2009.
- [10] Deepayan Bhowmik and Charith Abhayaratne. 2019. Embedding distortion analysis in wavelet-domain watermarking. *ACM Transactions on Multimedia Computing, Communications, and Applications* 15, 4 (2019), 24 pages.
- [11] D. M. Thodi and J. J. Rodriguez, "Expansion embedding techniques for reversible watermarking," *IEEE Trans. Image Process.*, vol. 16, no. 3, pp. 721–730, Mar. 2007.
- [12] J. Tian, "Reversible data embedding using a difference expansion," *IEEE Trans. Circuits Syst. Video Technol.*, vol. 13, no. 8, pp. 890–896, Aug. 2003.
- [13] Gouenou Coatrieux, Wei Pan, Nora Cuppens-Boulaiah, Frederic Cuppens, and Christian Roux. 2013. Reversible watermarking based on invariant image classification and dynamic histogram shifting. *IEEE Transactions on Information Forensics and Security* 8, 1 (2013), 111–120.
- [14] I. C. Dragoi and D. Coltuc. 2014. Local-prediction-based difference expansion reversible watermarking. *IEEE Transactions on Image Processing* 23, 4 (2014), 1779.
- [15] W. He and Z. Cai. 2020. An insight into pixel value ordering prediction-based prediction-error expansion. *IEEE Transactions on Information Forensics and Security* 15 (2020), 3859–3871.
- [16] Y. Q. Shi, X. Li, X. Zhang, H. T. Wu, and B. Ma. 2016. Reversible

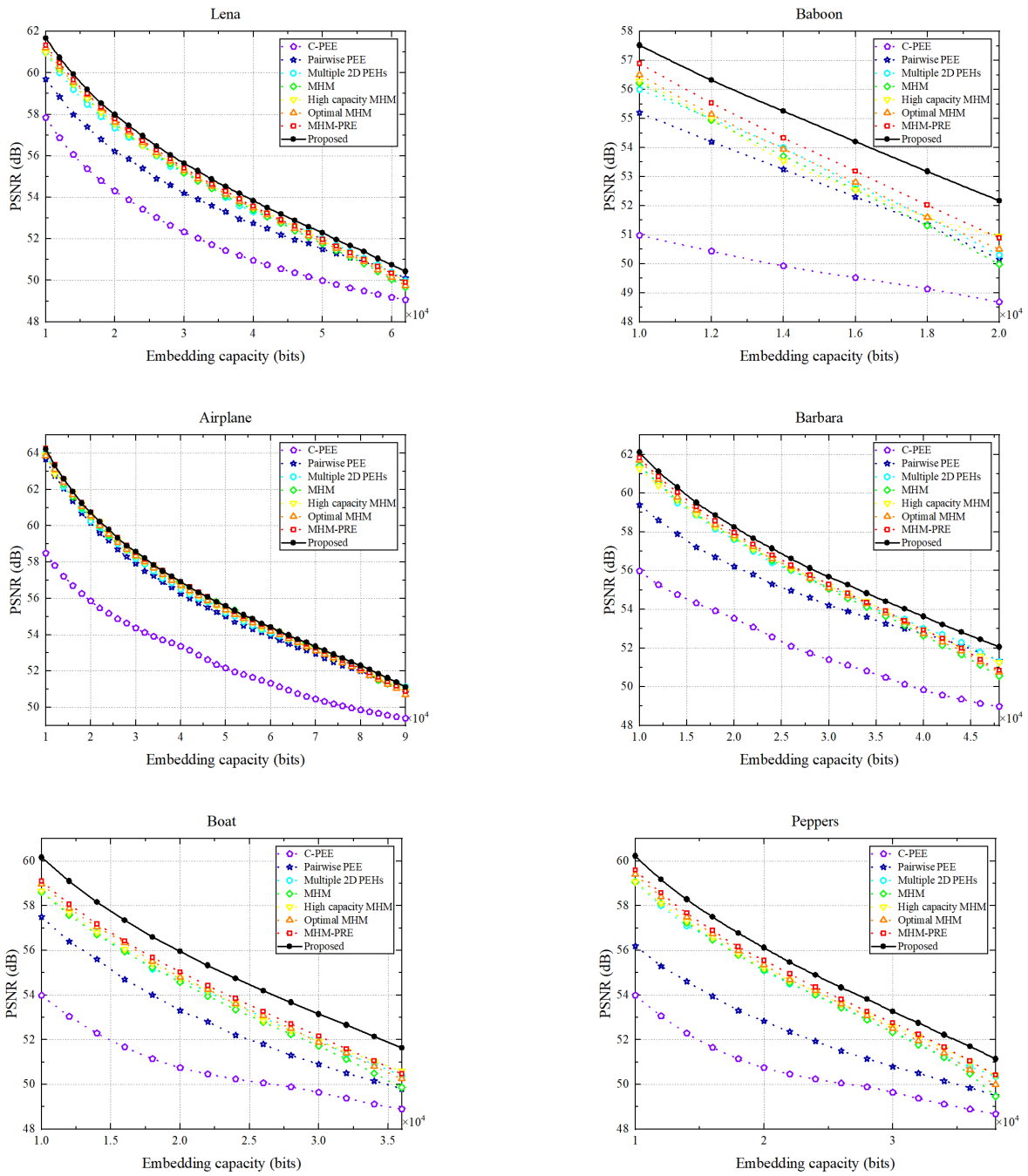


Fig. 14. Performance comparison between the proposed method and C-PEE, Pairwise PEE, MHM, MHM-based methods

TABLE IV

THE DETERMINED PARAMETERS $p_{t,b}$, $r_{t,b}$ ($0 \leq t \leq 2$, $-2 \leq b \leq 2$) OF OUR METHOD. FOR THE BLUE (FIRST LAYER EMBEDDING) AND YELLOW (SECOND LAYER EMBEDDING) PIXELS OF IMAGE LENA WITH 10,000 AND 20,000 EMBEDDING CAPACITIES

	EC = 10,000 bits		EC = 20,000 bits	
	blue	yellow	blue	yellow
$(p_{0,-2}, r_{0,-2})$	(-4, 6)	(-4, 3)	(-4, 2)	(-2, 1)
$(p_{0,-1}, r_{0,-1})$	(-2, 3)	(-4, 3)	(-2, 1)	(-2, 1)
$(p_{0,0}, r_{0,0})$	(-3, 2)	(-2, 2)	(-1, 1)	(-2, 2)
$(p_{0,1}, r_{0,1})$	(-2, 1)	(-3, 1)	(-1, 1)	(-2, 1)
$(p_{0,2}, r_{0,2})$	(-2, 2)	(-2, 3)	(-2, 2)	(-2, 1)
$(p_{1,-2}, r_{1,-2})$	(-2, 6)	(-3, 2)	(-2, 2)	(-2, 2)
$(p_{1,-1}, r_{1,-1})$	(-3, 2)	(-4, 3)	(-3, 2)	(-3, 2)
$(p_{1,0}, r_{1,0})$	(-5, 3)	(-4, 4)	(-3, 2)	(-4, 2)
$(p_{1,1}, r_{1,1})$	(-4, 4)	(-4, 5)	(-4, 2)	(-4, 2)
$(p_{1,2}, r_{1,2})$	(-3, 5)	(-3, 3)	(-2, 4)	(-3, 5)
$(p_{2,-2}, r_{2,-2})$	(-5, 3)	(-4, 8)	(-2, 2)	(-3, 2)
$(p_{2,-1}, r_{2,-1})$	(-4, 4)	(-6, 5)	(-4, 3)	(-3, 2)
$(p_{2,0}, r_{2,0})$	(-4, 4)	(-4, 4)	(-3, 3)	(-4, 3)
$(p_{2,1}, r_{2,1})$	(-4, 3)	(-3, 4)	(-4, 2)	(-3, 3)
$(p_{2,2}, r_{2,2})$	(-3, 2)	(-5, 5)	(-3, 2)	(-5, 2)

data hiding: Advances in the past two decades. IEEE Access 4 (2016), 3210–3237.

- [17] Ruchira Naskar and Rajat Subhra Chakraborty. 2013. A generalized tamper localization approach for reversible watermarking algorithms. ACM Transactions on Multimedia Computing, Communications, and Applications 9, 3 (2013), 22 pages.
- [18] H.-T. Wu and J. Huang, “Reversible image watermarking on prediction errors by efficient histogram modification,” Signal Process., vol. 92, no. 12, pp. 3000–3009, Dec. 2012.
- [19] C. Wang, X. Li, and B. Yang, “Efficient reversible image watermarking by using dynamical prediction-error expansion,” in Proc. IEEE ICIP, Sep. 2010, pp. 3673–3676.
- [20] V. Sachnev, H. J. Kim, J. Nam, S. Suresh, and Y. Q. Shi, “Reversible watermarking algorithm using sorting and prediction,” IEEE Trans. Circuits Syst. Video Technol., vol. 19, no. 7, pp. 989–999, Jul. 2009.
- [21] W. Hong, “An efficient prediction-and-shifting embedding technique for high quality reversible data hiding,” EURASIP J. Appl. Signal Process., vol. 2010, May 2010, Art. ID 104835.
- [22] X. Li, B. Yang, and T. Zeng, “Efficient reversible watermarking based on adaptive prediction-error expansion and pixel selection,” IEEE Trans. Image Process., vol. 20, no. 12, pp. 3524–3533, Dec. 2011.
- [23] W. Hong, “Adaptive reversible data hiding method based on error energy control and histogram shifting,” Opt. Commun., vol. 285, no. 2, pp. 101–108, Jan. 2012.
- [24] H. J. Hwang, H. J. Kim, V. Sachnev, and S. H. Joo, “Reversible watermarking method using optimal histogram pair shifting based on prediction and sorting,” KSII Trans. Internet Inf. Syst., vol. 4, no. 4, pp. 655–670, Aug. 2010.
- [25] G. Xuan, X. Tong, J. Teng, X. Zhang, and Y. Q. Shi, “Optimal histogram-pair and prediction-error based image reversible data hiding,” in Proc. IWDW, vol. 7809, 2012, pp. 368–383.
- [26] Bo Ou, Xiaolong Li, Yao Zhao, Rongrong Ni, and Yun-Qing Shi. 2013. Pairwise prediction-error expansion for efficient reversible data hiding. IEEE Transactions on Image Processing 22, 12 (2013), 5010–5021.
- [27] Vasilij Sachnev, Hyoung Joong Kim, Jeho Nam, Sundaram Suresh, and Yun Qing Shi. 2009. Reversible watermarking algorithm using sorting and prediction. IEEE Transactions on Circuits and Systems for Video Technology 19, 7 (2009), 989–999.
- [28] Mengyao Xiao, Xiaolong Li, Yao Zhao, Bin Ma, and Guodong Guo. 2023. A Novel Reversible Data Hiding Scheme Based on Pixel-Residual Histogram. ACM Trans. Multimedia Comput. Commun. Appl. 19, 1s, Article 46 (January 2023), 19 pages.